Oncolytic adenovirus Delta-24-RGD induces a widespread glioma proteotype remodeling during autophagy

Andrea González-Morales[1,2,3], Aintzane Zabaleta[2,4], Marc García-Moure[2,5,6], Marta M. Alonso[2,5,6], Joaquín Fernández-Irigoyen[1,2,3]§, Enrique Santamaría[1,2,3]§

[1] Clinical Neuroproteomics Group, Navarrabiomed, Complejo Hospitalario de Navarra (CHN), Universidad Pública de Navarra (UPNA), Irunlarrea 3. 31008 Pamplona, Spain; [2] IDISNA, Navarra Institute for Health Research, Pamplona, Spain; [3] Proteored-ISCIII, Proteomics Unit, Navarrabiomed, Complejo Hospitalario de Navarra (CHN), Universidad Pública de Navarra (UPNA), Irunlarrea 3. 31008 Pamplona, Spain; [4] Oncohematology Area, University Hospital of Navarra, Center for Applied Medical Research, CIBERONC, Pamplona, Spain. [5] Program in Solid Tumors and Biomarkers, Foundation for the Applied Medical Research, Pamplona, Spain; [6] Department of Pediatrics, University Hospital of Navarra, Pamplona, Spain.

§ These authors share senior authorship

Corresponding author: Enrique Santamaría, PhD. Proteomics Unit, Navarrabiomed, Navarra Institute for Health Research (IDISNA), Irunlarrea Street, 3 Pamplona, CP 31008 (Spain). Phone number: +(34) 848 42 57 40E-mail: esantamma@navarra.es.

Abbreviations

c-Src: proto-oncogene tyrosine-protein kinase Src

ERK1/2: extracellular signal–regulated kinase 1/2

GBM: glioblastoma

GSK-3: glycogen synthase kinase-3

MOI: Multiplicity of infection

MSK1/2: Mitogen- and Stress-activated protein Kinases 1 and 2

mpi: minutes post infection

hpi: hours post infection

p38 MAPK: p38 mitogen-activated protein kinase

PKA: Protein kinase A

PKC: Protein kinase C

PP1: serine/threonine-protein phosphatase 1

PP2A: serine/threonine-protein phosphatase 2A

Abstract

Adenovirus Delta-24-RGD has shown a remarkable efficacy in a phase I clinical trial for glioblastoma. Delta-24-RGD induces autophagy in glioma cells, however, the molecular derangements associated with Delta-24-RGD infection remains poorly understood. Here, proteomics was applied to characterize the glioma metabolic disturbances soon after Delta-24-RGD internalization and late in infection. Minutes post-infection, a rapid survival reprogramming of glioma cells was evidenced by an early c-Jun activation and a time-dependent dephosphorylation of multiple survival kinases. At 48 hours post-infection (hpi), a severe intracellular proteostasis impairment was characterized, detecting differentially expressed proteins related to mRNA splicing, cytoskeletal organization, oxidative response, and inflammation. Specific kinase-regulated protein interactomes for Delta-24-RGD-modulated proteome revealed interferences with the activation dynamics of protein kinases C and A (PKC, PKA), tyrosine-protein kinase Src (c-Src), glycogen synthase kinase-3 (GSK-3) as well as serine/threonine-protein phosphatases 1 and 2A (PP1, PP2A) at 48hpi, in parallel with adenoviral protein overproduction. Moreover, the late activation of the nuclear factor kappa B (NF-κB) correlates with the extracellular increment of specific cytokines involved in migration, and activation of different inflammatory cells. Taken together, our integrative analysis provides further insights into the effects triggered by Delta-24-RGD in the modulation of tumor suppression and immune response against glioma.

Keywords: Adenovirus, Delta-24RGD infection, proteomics, glioma, networks, signaling

1. Introduction

DNX-2401 (Delta-24-RGD) is an oncolytic adenovirus that replicates selectively in retinoblastoma (Rb) pathway deficient cells and infects tumor cells efficiently (*1-3*). In general, results from pre-clinical and clinical studies have revealed that the adenovirus Delta-24-RGD is an attractive therapeutic agent for malignant gliomas (*1*, *4-7*), demonstrating favorable toxicity profile and remarkable clinical efficacy (*8*). Indeed, novel clinical trials in combination with specific immunomodulators are currently active (Clinical-Trials.gov identifiers NCT02197169, and NCT02798406).

It is well-known that the mechanism of oncolytic Delta-24-RGD-mediated tumor suppression involves adenovirus-induced activation of the autophagic machinery in glioma cells (*9*). We consider that understanding the proteostatic changes associated with the viral cycle of Delta-24-RGD, will provide new avenues to enhance the capability of viral release, and, as a result, to elicit a more therapeutic effect. Using quantitative extracellular and intracellular proteomics workflows, physical and functional interaction data, and biochemical approaches, we have partially characterized the missing links in the biochemical understanding of the signaling pathways impaired during the initial phase of attachment and internalization of viral particles as well as during the autophagic phase of Delta-24-RGD infection (*10-13*). More than 200 differential proteins were detected in Delta-24-RGD-infected glioma cells, pinpointing protein interaction networks, specific pathways, and potential novel therapeutic targets. In addition, a specific increase in specific cytokine subsets was detected by extracellular cytokine profiling of glioma-infected cells, supporting the notion that Delta-24-RGD modulates pathways related to migration, and activation of different inflammatory cells.

2 Materials and methods

2.1 Materials

The following reagents and materials were used: anti-GAPDH (Calbiochem), anti-PKC-Pan, anti-pPKC-pan (T514), anti-pAkt (Ser473), anti-Akt, anti-cJUN, anti-phospho cJUN (S73), anti-NF-κB p65, anti-NF-κB phospho-p65 (S536), anti-IκB-alpha, anti-MEK, anti-pMEK (S217/221), anti-PKAc alpha, anti-pPKAc (T197), anti-GSK-3α/β, anti-pGSK-3α/β (S21/9) (Cell Signaling), anti-PP1, anti-c-src, anti-p-c-src (Y419), anti-E1A protein (Santa Cruz Biotechnology), anti-phospho PPP1A (T320), anti-PP2Aα/β (Abcam), and anti-fiber protein (Neomarkers). Electrophoresis reagents were purchased from Bio-rad and trypsin from Promega.

2.2 Virus production, culture and treatment of malignant glioma cells.

The generation of Delta-24-RGD vector has been previously described (*1, 3*). U87 MG glioma cells (ATCC: HTB-14) were cultured in DMEM/F12-GlutaMAX (Gibco 10565018) supplemented with 10% FBS, and 1% penicillin/streptomycin. $2.5x10^6$ U87 cells were infected with Delta-24-RGD at multiplicity of infection (MOI) of 25. After incubation for 30 minutes with DMEM/F12 1% penicillin/streptomycin at 37 °C, the double of the volume of DMEM/F12-GlutaMAX (Gibco 10565018) supplemented with 10% FBS and 1% penicillin and streptomycin was added to the previous media. Cells were incubated under the same conditions during the indicated periods of time (24 and 48hpi).

2.3 Mass-spectrometry based-proteomics

After the indicated periods of time, the media was removed and the cells were washed with 1X cold PBS. The cellular pellets were resuspended in lysis buffer (7M urea, 2M thiourea, 50mM DTT) and let on ice for 30 minutes, spinning and vortexing each 10 minutes. After a sonication step, the lysate was centrifuged for 60 minutes at 20000xg at 15°C. Protein concentration of the supernatants was measured with the Bradford assay

kit (Bio-rad). Total cell extracts from Mock-infected, and U87-infected cells (48hpi) were diluted in Laemmli sample buffer and loaded into a 1 mm thick polyacrylamide gel with a 4% stacking gel casted over a 12.5% resolving gel. The run was stopped as soon as the front entered 3 mm into the resolving gel so that the whole proteome became concentrated in the stacking/resolving gel interface. Bands were stained with Coomassie Brilliant Blue and excised from the gel. Protein enzymatic cleavage (15ug) was carried out with trypsin (Promega; 1:20, w/w) at 37°C for 16 h. Purification and concentration of peptides was performed using C18 Zip Tip Solid Phase Extraction (Millipore). Peptides mixtures were separated by reverse phase chromatography as previously described (*26*). The column gradient was developed in a 240 min two step gradient from 5% B to 25% B in 210 min and 25%B to 40% B in 30 min. Column was equilibrated in 95% B for 9 min and 5% B for 14 min. During all processes, precolumn was in line with column and flow maintained all along the gradient at 300 nl/min. Eluting peptides from the column were analyzed using a Sciex 5600 Triple-TOF system. Information data acquisition was acquired upon a survey scan performed in a mass range from 350 m/z up to 1250 m/z in a scan time of 250 ms. Top 25-35 peaks were selected for fragmentation. Product ions were scanned in a mass range from 230 m/z up to 1500 m/z and excluded for further fragmentation during 15 s. The MS/MS data acquisition was performed using Analyst 1.7.1 (Sciex) and spectra files were processed through Protein Pilot Software (v.5.0.1-Sciex) using Paragon™ algorithm (v.5.0.1) for database search, Progroup™ for data grouping, and searched against the concatenated target-decoy UniProt proteome reference database (Human database Proteome ID: UP000005640, 70902 proteins, December 2015 plus adenovirus HAv5 database UP000004992, 31 proteins, September 2016). False discovery rate was performed using a non-lineal fitting method and displayed results were those reporting a 1% Global false discovery rate or better. The mass spectrometry proteomics data have

been deposited to the ProteomeXchange Consortium (http://proteomecentral.proteomexchange.org) (*55*) via the PRIDE partner repository with the data set identifier PXD010256.

(For reviewers, Username: reviewer37737@ebi.ac.uk; Password: IVLEQLmD)

2.4 Data analysis

The peptide quantification was performed using the Progenesis LC−MS software (ver. 2.0.5556.29015, Nonlinear Dynamics). Using the accurate mass measurements from full survey scans in the TOF detector and the observed retention times, runs were aligned to compensate for between-run variations in our nanoLC separation system. To this end, all runs were aligned to a reference run automatically chosen by the software, and a master list of features considering m/z values and retention times was generated. The quality of these alignments was manually supervised with the help of quality scores provided by the software. The peptide identifications were exported from Protein Pilot software and imported in Progenesis LC− MS software where they were matched to the respective features. Output data files were managed for subsequent statistical analyses and representation. Proteins identified by site (identification based only on a modification), reverse proteins (identified by decoy database) and potential contaminants were filtered out. Proteins quantified with at least two unique peptides, a T-test p-value lower than 0.05, and an absolute fold change of <0.77 (down-regulation) or >1.3 (up-regulation) in linear scale were considered significantly differentially expressed.

2.5 Bioinformatics

The proteomic data were analyzed using STRING (*56*) and QIAGEN's Ingenuity® Pathway Analysis (IPA) (QIAGEN Redwood City, www.qiagen.com/ingenuity), to detect and infer differentially activated/deactivated pathways because of Delta-24RGD treatment. STRING database includes interactions from published literature describing

experimentally studied interactions, as well as those from genome analysis using several well-established methods based on domain fusion, phylogenetic profiling and gene neighbourhood concepts. Accordingly, a confidence score for every protein–protein association was assigned to the network. A higher score was assigned when an association is supported by several types of evidence. To minimize false positives as well as false negatives, all interactions tagged as "low-confidence" (<0.4) in STRING database have been eliminated from this study. IPA software comprises curated information from databases of experimental and predictive origin, enabling discovery of highly represented functions, pathways, and interactome networks. The IPA comparison analysis considers the signalling pathway rank according to the calculated p-value and reports it hierarchically. The software generates significance values (p-values) between each biological or molecular event and the imported molecules based on the Fisher´s exact test ($p \leq 0.05$).

2.6 Protein arrays

For the secretome analysis, a dot-blot protein array was used for cytokine profiling (Abcam). Briefly, membranes with 80 cytokine antibodies were blocked with the manufacturer's blocking buffer at room temperature (RT) for 30 min, and incubated o/n with 1ml of undiluted cell-cultured media from Mock- and U87-infected cells (24, 48hpi) (n=3). After washing, a biotinylated anti-cytokine antibody mixture was added to the membranes followed by incubation with HRP-conjugated streptavidin and then exposed to the manufacturer's peroxidase substrate. For phospho-kinome analysis, the Proteome Profiler Array (R&D Systems. Ref: 894552) was used according to the manufacturer instructions. Cell lysates derived from Mock- and U87-infected cells (5, 15, 30 mpi) (n=3) were diluted and incubated overnight with the Human Phospho-Kinase Array, that contains 43 different capture antibodies printed in duplicate. The arrays were washed to

remove unbound proteins followed by incubation with a cocktail of biotinylated detection antibodies. Streptavidin-HRP and chemiluminescent detection reagents were applied and a signal was produced at each capture spot corresponding to the amount of phosphorylated protein bound. For both protein array platforms, chemiluminescence signals were quantified with the ImageQuant ECL system (BioRad) and normalized to the positive control signals. The Perseus software (version 1.5.6.0) was used for statistical analysis (*57*).

2.7 Western-blotting

Equal amounts of protein (10 µg) were resolved in 4–15% Criterion™ TGX Stain-Free™ Protein Gels (#5678085 Bio-rad). Mock-infected and U87-infected protein cell extracts were electrophoretically transferred onto nitrocellulose membranes using Trans-Blot Turbo (BioRad) for 7 minutes at 2.5A constant, up to 25V. Equal loading of the gels was assessed by stain free digitalization and Ponceau staining. Membranes were probed with primary antibodies at 1:1000 dilution in 5% nonfat milk or BSA. After incubation with the appropriate horseradish peroxidase-conjugated secondary antibody (1:5000), antibody binding was detected by a Chemidoc™MP Imaging System (Bio-Rad) after incubation with an enhanced chemiluminescence substrate (Perkin Elmer). All Band intensities were measured with Image Lab Software Version 5.2 (Bio-Rad), and normalized to GAPDH or to total stain in each gel lane (*58*).

3. Results and discussion

Glioblastoma multiforme (GBM) is the most aggressive type of malignant glioma, characterized by infiltrative growth causing progressive neurologic dysfunction (*14*). One of the treatment strategies currently used is the oncolytic virotherapy (*15, 16*), that combines tumoral cell lysis with systemic anti-tumor immunity induction. Delta-24-RGD, also known as DNX-2401, is currently under investigation in clinical trials for

GBM (*8*). However, the global molecular events that accompany the adenoviral infective process remain to be elucidated. We consider that a system-wide characterization of initial phosphoproteomic events as well as the intracellular and extracellular glioma proteomes underlying the regulation of autophagy upon Delta-24-RGD infection (Figure 1) may provide new inducing or inhibiting strategies to improve the therapeutic effect against target glioma cells.

3.1 Delta-24-RGD-receptor interactions rapidly modulate the glioma phosphoproteome

To identify signaling events induced soon after Delta-24-RGD engagement of cell surface receptors, phospho-kinase arrays were performed at 5, 15, and 30 minutes post-infection (mpi). To synchronize virus binding, we added a high concentration of virus (MOI=25) in order to obtain a sufficient number of binding events within a very short time-frame. As shown in figure 2, a time-dependent dephosphorylation of specific survival routes was observed (Akt, GSK-3, ERK1/2, p38 MAPK, MSK1/2 between others), indicating that Delta-24-RGD induces an early survival reprogramming of glioma cells for an optimal viral replication. Akt was progressively inactivated during the time-points analysed (Figure 2A-B). Phospho-WNK-1 (T60), an Akt substrate implicated in regulating ion permeability (*17, 18*) was also dephosphorylated during the first 30 mpi (Figure 2A-B). Interestingly, the activation of WNK-1/OSR1/NKCC1 signaling pathway facilitates glioma cell migration and apoptotic resistance to the chemotherapeutic drug temozolomide (TMZ) (*19*), reinforcing the idea that co-treatment of glioma cells with TMZ and Delta-24-RGD might lead to an enhanced therapeutic effect (*20*). c-Jun was the unique factor that rapidly increased its activator phosphorylation (Figure 2A-B). Although Jun N-terminal kinases (JNKs) are the canonical regulator of c-Jun activity (*21, 22*), a JNK activation was not observed at 5-15 mpi (Figure 2C-D), indicating that additional kinases (*23*) may be responsible for the c-Jun early activation peak during

Delta-24-RGD attachment. Together with the shut off induced in the kinase-mediated signaling, several transcription factors were rapidly inhibited (30mpi) such as STAT2 and STAT5b (figure 2C-D), probably blocking the antiviral defense (*24*), causing cycle arrest, and inhibiting glioma cell growth (*25*).

3.2 Delta-24-RGD induces protein interactome derangements late in infection

It is well known that for an efficient cell lysis and adenoviral spread, Delta-24-RGD induces massive autophagy (*10-12*). We have determined the Delta-24-RGD-induced glioma proteome remodelling that occurs in parallel with the overproduction viral proteins and the concomitant activation of Akt and c-Jun at 48hpi (*9*) (Figure 3A). Among the 1616 intracellular proteins consistently quantified (figure 3B and supplementary table 1), 240 proteins tend to be differentially expressed between Mock and glioma-infected cells (127 up-regulated, and 113 down-regulated proteins) (figure 3B and Supplementary table 2), being potentially distributed across nuclear, cytosolic, exosome, and membranes between other organelles (Figure 3C). In addition, the over-production of 18 adenoviral proteins was also detected by mass-spectrometry (supplementary table 2). In accordance with previous studies (*9, 26*), Delta-24-RGD modulates proteomic fingerprints involved in EIF2 and mTOR signalling (figure 3D). Changes in the expression of various autophagy-related biomarker proteins were also detected in our proteomic survey. p62 (SQSTM1) down-regulation was evidenced in Delta-24-RGD-infected glioma cells. This molecular event is a marker of autophagy in oncolytic adenovirus-infected tumor cells, where p62 may act as a receptor for ubiquitinated proteins or organelles (*27*), being finally degraded by the autolysosome (*28*). The autophagosome-lysosome fusion requires the lysosomal membrane protein LAMP-2 (*27*), an over-expressed protein in Delta-24-RGD-infected cells. Moreover, cytoskeleton organization (RhoA signaling, ILK signaling), inflammation (IL-8 signaling), oxidative response, and differentiation (Tec kinase

signalling, HGF and integrin signalling) were disrupted biological functions that accompanied Delta-24-RGD-mediated autophagy (figure 3D). Interestingly, deregulated proteins involved in protein synthesis (Ribosome biogenesis protein BOP1, 60S acidic ribosomal protein P2, 40S ribosomal protein S23) and DNA/RNA metabolism (TATA-binding protein-associated factor 2N, DNA-directed RNA polymerases I and III subunit RPAC1, DNA replication licensing factor MCM4, Cleavage stimulation factor subunit 3, and RNA-binding protein FUS) at 48 hpi, have been previously proposed as Delta-24-RGD targets early in infection (*26*). To characterize in detail the glioma proteotype upon Delta-24-RGD infection in the autophagic stage, we have performed proteome-scale interaction networks merging the 240 differential proteins detected in glioma-infected cells (48 hpi) (Figure 4). The protein interactome was mainly composed by specific protein clusters related to Poly(A) RNA binding, translation, mRNA splicing, and AMP metabolism. As shown in figure 4, Delta-24-RGD treatment directly affects the protein tyrosine kinase signalling, highly associated with glioblastoma oncogenesis (*29*).

3.3 Activation state of predictive interactome hubs upon Delta-24-RGD infection

We have applied a system biology approach to establish a framework to monitor interaction between deregulated proteins and potential network modules that may be considered as protein targets to modulate the infectivity process. Akt and JNK appeared as functional interactors of part of the deregulated proteome (supplementary file 3), being activated during Delta-24-RGD mediated autophagy (*9*). As shown in figure 5, NFκB also appeared as a hub in the differential interactome network. Subsequent experiments were performed to monitor the activation state of this signal transducer late in infection (Figure 5A). The increment in the serine 536 pohosphorylation of NFκB (24-48hpi) and the drop in the levels of the NFκB inhibitor alpha (IκB-alpha) at 48hpi suggests a potential activation of this transcription factor. Previous studies point out that adenovirus infection

induces the activation of NF-κB in cancer cell lines (*30, 31*), being associated with resistance to different cell death and chemotherapeutic strategies in GBM (*32*), suggesting that Delta-24-RGD-induced NF-κB activation might be a protection mechanism induced by glioma cells. PKC isozymes are overexpressed in astroglial brain tumors (*33*). Our data indicate that Delta-24-RGD decreases PKC protein levels (Figure 5B), probably restraining the hyperproliferative state and the invasive capacity of malignant glioma cells (*34*). Despite src kinase is also frequently activated in GBM, the use of specific inhibitory strategies has demonstrated a reduction in cell viability, and migration (*35*) as well as an induction of autophagic cell death in GBM cells (*36*). As shown in figure 5B, the essential phosphorylation of Y419 in the activation loop of c-src (*37*), and total c-src levels were markedly reduced in glioma-infected cells at 48hpi (Figure 5B). Moreover, Delta-24-RGD also affects the MAPK pathway, as suggested by the down-regulation of ERK (Supplementary table 2) and its target MEK1/2 (figure 6A). All these data point out that Delta-24-RGD treatment directly interferes with signaling pathways involved in cell growth, proliferation, adhesion, and migration. Due to the reduction of PKA type 1a regulatory subunit (PRKAR1A) in Delta-24-RGD-infected cells (Supplementary Table 2, network figure 6A), we focus our attention in the potential deregulation of PKA activation. As shown in figure 6A, an increment in phosphorylated and total PKA levels was evidenced at 24hpi. Being PKA an E1A adenoviral protein interactor, the co-overexpression of both proteins observed at 24hpi may contribute to viral transcription, protein expression and progeny production (*38*). However, PKA activation was reduced at 48hpi (figure 6A). This PKA inhibition was supported by the down-regulation of Ras GTPase-activating protein 1 (RASA1), an inhibitory regulator of the Ras-cyclic AMP pathway, that compromises cAMP generation.

A growing body of evidences indicates that total and phosphorylated GSK-3 levels are increased in GBM, influencing its malignant phenotype (*39*). As shown in figure 6A, a dephosphorylation of GSK3α/β was observed at 24hpi, while GSK3α/β protein levels tend to be reduced at 48hpi. Although targeting of PKA and GSK-3 activity may result in glioma conventional cell death (*40-42*), PKA inhibition and GSK-3 down-regulation could also contribute to Delta-24-RGD-induced autophagic flux in glioma cells (*27, 43*). On the other hand, Delta-24-RGD also targeted serine/threonine protein phosphatase homeostasis in glioma cells late in infection. Specifically, Delta-24-RGD induced the overproduction of serine/threonine-protein phosphatase 6 catalytic subunit (PPP6C), PP4 regulatory subunit 3A (PPP4R3A) and PP1-beta catalytic subunit (PPP1CB) (Supplementary table 2). All of them have been previously related to glioblastoma invasion and recurrence (*44*). Figure 6B shows the PP1/PP2A-regulated interactome modulated by Delta-24-RGD. Despite the slight PP1- α catalytic subunit activation (by dephosphorylation) observed at 24hpi in infected-glioma cells, Delta-24-RGD induced a decrease in PP1α subunit and PP2A α/β catalytic subunit protein levels at 48hpi (figure 6B). Both S/T phosphatases are adenoviral E4orf4 protein interactors (*45, 46*) and cooperating partners in modulating the mitotic progression and tumor growth (*47, 48*), although a duality in the GBM field exists because PP2A inhibition or activation appear to be anti-oncogenic (*44*). Other protein that takes part in the PP1/PP2A-regulated interactome, is calreticulin (CALR), which expression is induced during Delta-24-RGD infection (figure 6B, and supplementary table 2). Interestingly, this protein is a damage-associated molecular pattern (DAMP) molecule involved in the induction of antitumor immune response during antitumor therapy-induced autophagy (*49, 50*).

3.4 Delta-24-RGD triggers changes in the glioma secretome late in infection

Based on cerebrospinal fluid analysis derived from GBM patients, Delta-24-RGD therapy alters the tumor microenvironment (*51*). Considering that the monitorization of cytokines and growth factors specifically secreted by glioma cells to the tumor microenvironment may provide new insights into the modulation of the immune response induced by Delta-24-RGD, we have performed a complementary secretome analysis of infected-glioma cells at 24 and 48hpi. Among the 80 secreted cell–cell signaling molecules analyzed, 14 were significantly increased in a time-dependent manner (Figure 7A). TGF-beta3 was significantly increased at 24 hpi whereas the chemotactic factor GRO (CXCL1), TIMP-1, and TIMP-2 were up-regulated at 24-48 hpi. Other cytoquines such as GM-CSF, IL-8 (CXCL8), angiogenin, BLC (CXCL13), HGF, IGFBP-1, MIF, osteopontin, and osteoprotegerin (TNFRSF11B) were specifically overproduced at 48 hpi (Figure 7A). Some of this cytokine and growth factors (GM-CSF, CXCL1, CXCL8, TIMP-1, TIMP-2, TNFRSF11B) are targets of the NFκB complex. These data indicated that the cytokine secretion waves induced by Delta-24-RGD are highly dynamic and time-dependent during all phases of Delta-24-RGD viral cycle (*26*). To explore the cooperative action among differentially intracellular and extracellular molecules induced by Delta-24-RGD at 48hpi, we have performed additional pathway analysis merging the proteomic dataset and the secretome information. As shown in figure 7B, Delta-24-RGD modulates pathways related to accumulation, migration, and activation of different inflammatory cells late in infection (supplementary table 4). It has been previously reported that Delta-24-RGD induces a prolonged shift in the pro-tumoral M2 macrophages towards tumor-detrimental phenotype as well as leukocyte recruitment and activation in GBM patients (*51*). All these data complement the notion that the immune system plays a fundamental role in the therapeutic efficacy of oncolytic Delta-24-RGD therapy of glioma (*52-54*).

4. Conclusion

This work provides new insights regarding the molecular mechanisms governing the glioma metabolism during Delta-24-RGD oncolytic adenoviral therapy. Although additional experiments are needed to evaluate the effect of Delta-24-RGD in additional cell lines and *in vivo* models, the application of high-throughput proteomic approaches proves to be a useful tool to decipher the proteome expression profiles of glioma cells during antitumor therapy, and more importantly, to define potential therapeutic targets against GBM.

Figure legends

Figure 1. Spatio-temporal multi-omic approach applied throughout Delta-24-RGD Infection.

Figure 2. Rapid phospho-kinome response of Delta-24-RGD-infected cells during the first 30 minutes of infection. Phosphoproteome variations detected at 5, 15, and 30 mpi respect to mock-infected cells (A, C). Representative images of phospho-kinase arrays are shown (B, D).

Figure 3. Differentially expressed proteins throughout late phases of Delta-24-RGD Infection. A) Expression of adenoviral proteins in glioma-infected cells. B) Volcano plot representing the fold-change of identified proteins with associated P values from the pair-wise quantitative comparison of mock vs glioma-infected proteome at 48hpi (Left). In green, significantly down-regulated proteins, and in red, upregulated proteins ($P < 0.05$). (C) Subcellular and (D) pathway distribution of the glioma proteome modulated by Delta-24-RGD (48hpi).

Figure 4. Protein interactome network for Delta-24-RGD-modulated proteome. Network analysis was performed submitting the corresponding protein IDs to the

STRING (Search Tool for the Retrieval of Interacting Genes) software (v.10.5) (http://stringdb.org/). Proteins are represented with nodes and the interactions with continuous lines to represent direct interactions (physical), while indirect ones (functional) are presented by interrupted lines. All the edges were supported by at least a reference from the literature or from canonical information stored in the STRING database. To minimize false positives as well as false negatives, only interactions tagged as "high confidence" (>0.7) in STRING database were considered. K means clustering was applied.

Figure 5. Delta-24-RGD-modulated proteome is functionally related with NFκB, SRC, and PKC. Specific protein interactomes modulated by Delta-24-RGD in glioma cells late in infection (48hpi) (down- and up-regulated proteins in Delta-24-RGD-infected glioma cells in green and red respectively). Levels and residue-specific phosphorylation of NFκB and IκB (A), PKC, and c-SRC (B) at 24-48hpi. Equal loading of the gels was assessed by Ponceau staining and band intensities were normalized to total stain in each gel lane. Representative Western blot images from three independent experiments are shown.

Figure 6. Delta-24-RGD induces specific signaling derangements late in infection. Specific kinase-regulated interactomes modulated by Delta-24-RGD in glioma cells at 48hpi (down- and up-regulated proteins in Delta-24-RGD-infected glioma cells in green and red respectively). Levels and residue-specific phosphorylation of PKAc, MEK1/2, and GSK3-□/□ (A), PP1α, and PP2A✔/🚲 (B) at 24-48hpi. Equal loading of the gels was assessed by Ponceau staining and band intensities were normalized to total stain in each gel lane. Representative Western blot images from three independent experiments are shown.

Figure 7. Delta 24-RGD induces late changes in the extracellular cytokine profiling of glioma cells. A time-dependent analysis of 80 cytokines/growth factors was performed in the cell media of mock-infected glioma cells and glioma-infected cells (24, and 48hpi) using a dot-blot protein array method. Three independent experiments were performed. Data are presented as mean ± SEM. *p < 0.05, **p<0.01, and ***p<0.001 vs mock-infected condition (A). Pathway mapping of intracellular deregulated proteins and the differential secretome obtained by IPA software (supplementary table 4) (B).

Supporting information

Additional file 1. Glioma proteome quantitation in Delta-24-RGD-infected cells (48hpi).

Additional file 2. Delta24RGD-modulated proteome in infected-glioma cells (48hpi).

Additional file 3. Protein interactomes deregulated by Delta-24-RGD. Akt and c-Jun activation late in infection.

Additional file 4. Pathway mapping of intracellular and extracellular proteins differentially expressed upon Delta-24-RGD infection.

Acknowledgements

This work was funded by grants from the Spanish Ministry of Economy and Competitiveness (MINECO) (Ref. SAF2014-59340-R To ES), the Department of Economic Development from Government of Navarra (Ref. PC023-PC024, PC025, PC081-82 and PI059 to ES and PI031 to JFI), the Instituto de Salud Carlos III and Fondos Feder Europeos (PI16/00066 to MMA), the Spanish Ministry of Science and Innovation (IEDI-2015-00638 to MMA), the Department of Health of the Government of Navarra (to MMA), the Basque Foundation for Health Research (BIOEF, BIO13/CI/005 to MMA), Asociación Pablo Ugarte-Fuerza, Julen (to MMA). AGM was supported by PEJ-2014-A-61949 (MINECO). Authors thank all PRIDE Team for helping with the mass

spectrometric data deposit in ProteomeXChange/PRIDE. The Proteomics Unit of Navarrabiomed is a member of Proteored, PRB3-ISCIII, and is supported by grant PT17/0019/0009, of the PE I+D+I 2013-2016 funded by ISCIII and FEDER.

References

1. Fueyo, J., Alemany, R., Gomez-Manzano, C., Fuller, G. N., Khan, A., Conrad, C. A., Liu, T. J., Jiang, H., Lemoine, M. G., Suzuki, K., Sawaya, R., Curiel, D. T., Yung, W. K., and Lang, F. F. (2003) Preclinical characterization of the antiglioma activity of a tropism-enhanced adenovirus targeted to the retinoblastoma pathway, *J Natl Cancer Inst 95*, 652-660.
2. Fueyo, J., Gomez-Manzano, C., Alemany, R., Lee, P. S., McDonnell, T. J., Mitlianga, P., Shi, Y. X., Levin, V. A., Yung, W. K., and Kyritsis, A. P. (2000) A mutant oncolytic adenovirus targeting the Rb pathway produces anti-glioma effect in vivo, *Oncogene 19*, 2-12.
3. Suzuki, K., Fueyo, J., Krasnykh, V., Reynolds, P. N., Curiel, D. T., and Alemany, R. (2001) A conditionally replicative adenovirus with enhanced infectivity shows improved oncolytic potency, *Clin Cancer Res 7*, 120-126.
4. Jiang, H., Clise-Dwyer, K., Ruisaard, K. E., Fan, X., Tian, W., Gumin, J., Lamfers, M. L., Kleijn, A., Lang, F. F., Yung, W. K., Vence, L. M., Gomez-Manzano, C., and Fueyo, J. (2014) Delta-24-RGD oncolytic adenovirus elicits anti-glioma immunity in an immunocompetent mouse model, *PLoS One 9*, e97407.
5. Jiang, H., Gomez-Manzano, C., Aoki, H., Alonso, M. M., Kondo, S., McCormick, F., Xu, J., Kondo, Y., Bekele, B. N., Colman, H., Lang, F. F., and Fueyo, J. (2007) Examination of the therapeutic potential of Delta-24-RGD in brain tumor stem cells: role of autophagic cell death, *J Natl Cancer Inst 99*, 1410-1414.
6. Jiang, H., Gomez-Manzano, C., Lang, F. F., Alemany, R., and Fueyo, J. (2009) Oncolytic adenovirus: preclinical and clinical studies in patients with human malignant gliomas, *Curr Gene Ther 9*, 422-427.
7. Tejada, S., Alonso, M., Patino, A., Fueyo, J., Gomez-Manzano, C., and Diez-Valle, R. (2017) Phase I Trial of DNX-2401 for Diffuse Intrinsic Pontine Glioma Newly Diagnosed in Pediatric Patients, *Neurosurgery*.
8. Lang, F. F., Conrad, C., Gomez-Manzano, C., Yung, W. K. A., Sawaya, R., Weinberg, J. S., Prabhu, S. S., Rao, G., Fuller, G. N., Aldape, K. D., Gumin, J., Vence, L. M., Wistuba, I., Rodriguez-Canales, J., Villalobos, P. A., Dirven, C. M. F., Tejada, S., Valle, R. D., Alonso, M. M., Ewald, B., Peterkin, J. J., Tufaro, F., and Fueyo, J. Phase I Study of DNX-2401 (Delta-24-RGD) Oncolytic Adenovirus: Replication and Immunotherapeutic Effects in Recurrent Malignant Glioma, *J Clin Oncol 36*, 1419-1427.
9. Klein, S. R., Piya, S., Lu, Z., Xia, Y., Alonso, M. M., White, E. J., Wei, J., Gomez-Manzano, C., Jiang, H., and Fueyo, J. (2015) C-Jun N-terminal kinases are required for oncolytic adenovirus-mediated autophagy, *Oncogene 34*, 5295-5301.

10. Ito, H., Aoki, H., Kuhnel, F., Kondo, Y., Kubicka, S., Wirth, T., Iwado, E., Iwamaru, A., Fujiwara, K., Hess, K. R., Lang, F. F., Sawaya, R., and Kondo, S. (2006) Autophagic cell death of malignant glioma cells induced by a conditionally replicating adenovirus, *J Natl Cancer Inst 98*, 625-636.
11. Jiang, H., White, E. J., Gomez-Manzano, C., and Fueyo, J. (2008) Adenovirus's last trick: you say lysis, we say autophagy, *Autophagy 4*, 118-120.
12. Jiang, H., White, E. J., Rios-Vicil, C. I., Xu, J., Gomez-Manzano, C., and Fueyo, J. (2011) Human adenovirus type 5 induces cell lysis through autophagy and autophagy-triggered caspase activity, *J Virol 85*, 4720-4729.
13. Piya, S., White, E. J., Klein, S. R., Jiang, H., McDonnell, T. J., Gomez-Manzano, C., and Fueyo, J. (2011) The E1B19K oncoprotein complexes with Beclin 1 to regulate autophagy in adenovirus-infected cells, *PLoS One 6*, e29467.
14. Bianco, J., Bastiancich, C., Jankovski, A., des Rieux, A., Preat, V., and Danhier, F. (2017) On glioblastoma and the search for a cure: where do we stand?, *Cell Mol Life Sci 74*, 2451-2466.
15. Lawler, S. E., Speranza, M. C., Cho, C. F., and Chiocca, E. A. Oncolytic Viruses in Cancer Treatment: A Review, *JAMA Oncol 3*, 841-849.
16. Panek, W. K., Kane, J. R., Young, J. S., Rashidi, A., Kim, J. W., Kanojia, D., and Lesniak, M. S. Hitting the nail on the head: combining oncolytic adenovirus-mediated virotherapy and immunomodulation for the treatment of glioma, *Oncotarget 8*, 89391-89405.
17. Vitari, A. C., Deak, M., Collins, B. J., Morrice, N., Prescott, A. R., Phelan, A., Humphreys, S., and Alessi, D. R. (2004) WNK1, the kinase mutated in an inherited high-blood-pressure syndrome, is a novel PKB (protein kinase B)/Akt substrate, *Biochem J 378*, 257-268.
18. Choate, K. A., Kahle, K. T., Wilson, F. H., Nelson-Williams, C., and Lifton, R. P. (2003) WNK1, a kinase mutated in inherited hypertension with hyperkalemia, localizes to diverse Cl- -transporting epithelia, *Proc Natl Acad Sci U S A 100*, 663-668.
19. Zhu, W., Begum, G., Pointer, K., Clark, P. A., Yang, S. S., Lin, S. H., Kahle, K. T., Kuo, J. S., and Sun, D. WNK1-OSR1 kinase-mediated phospho-activation of Na+-K+-2Cl- cotransporter facilitates glioma migration, *Mol Cancer 13*, 31.
20. Alonso, M. M., Gomez-Manzano, C., Bekele, B. N., Yung, W. K., and Fueyo, J. (2007) Adenovirus-based strategies overcome temozolomide resistance by silencing the O6-methylguanine-DNA methyltransferase promoter, *Cancer Res 67*, 11499-11504.
21. Hibi, M., Lin, A., Smeal, T., Minden, A., and Karin, M. (1993) Identification of an oncoprotein- and UV-responsive protein kinase that binds and potentiates the c-Jun activation domain, *Genes Dev 7*, 2135-2148.
22. Derijard, B., Hibi, M., Wu, I. H., Barrett, T., Su, B., Deng, T., Karin, M., and Davis, R. J. (1994) JNK1: a protein kinase stimulated by UV light and Ha-Ras that binds and phosphorylates the c-Jun activation domain, *Cell 76*, 1025-1037.
23. Cho, Y. Y., Tang, F., Yao, K., Lu, C., Zhu, F., Zheng, D., Pugliese, A., Bode, A. M., and Dong, Z. (2009) Cyclin-dependent kinase-3-mediated c-Jun phosphorylation at Ser63 and Ser73 enhances cell transformation, *Cancer Res 69*, 272-281.

24. Blaszczyk, K., Nowicka, H., Kostyrko, K., Antonczyk, A., Wesoly, J., and Bluyssen, H. A. The unique role of STAT2 in constitutive and IFN-induced transcription and antiviral responses, *Cytokine Growth Factor Rev 29*, 71-81.
25. Liang, Y., Diehn, M., Watson, N., Bollen, A. W., Aldape, K. D., Nicholas, M. K., Lamborn, K. R., Berger, M. S., Botstein, D., Brown, P. O., and Israel, M. A. (2005) Gene expression profiling reveals molecularly and clinically distinct subtypes of glioblastoma multiforme, *Proc Natl Acad Sci U S A 102*, 5814-5819.
26. Gonzalez-Morales, A., Zabaleta, A., Guruceaga, E., Alonso, M. M., Garcia-Moure, M., Fernandez-Irigoyen, J., and Santamaria, E. Spatial and temporal proteome dynamics of glioma cells during oncolytic adenovirus Delta-24-RGD infection, *Oncotarget 9*, 31045-31065.
27. He, C., and Klionsky, D. J. (2009) Regulation mechanisms and signaling pathways of autophagy, *Annu Rev Genet 43*, 67-93.
28. Tazawa, H., Kuroda, S., Hasei, J., Kagawa, S., and Fujiwara, T. Impact of Autophagy in Oncolytic Adenoviral Therapy for Cancer, *Int J Mol Sci 18*.
29. Wick, W., Weller, M., Weiler, M., Batchelor, T., Yung, A. W., and Platten, M. Pathway inhibition: emerging molecular targets for treating glioblastoma, *Neuro Oncol 13*, 566-579.
30. Hodzic, J., Sie, D., Vermeulen, A., and van Beusechem, V. W. (2017) Functional Screening Identifies Human miRNAs that Modulate Adenovirus Propagation in Prostate Cancer Cells, *Hum Gene Ther 28*, 766-780.
31. Palmer, D. H., Chen, M. J., Searle, P. F., Kerr, D. J., and Young, L. S. (2005) Inhibition of NF-kappaB enhances the cytotoxicity of virus-directed enzyme prodrug therapy and oncolytic adenovirus cancer gene therapy, *Gene Ther 12*, 1187-1197.
32. Nogueira, L., Ruiz-Ontanon, P., Vazquez-Barquero, A., Moris, F., and Fernandez-Luna, J. L. (2011) The NFkappaB pathway: a therapeutic target in glioblastoma, *Oncotarget 2*, 646-653.
33. Sharif, T. R., and Sharif, M. (1999) Overexpression of protein kinase C epsilon in astroglial brain tumor derived cell lines and primary tumor samples, *Int J Oncol 15*, 237-243.
34. da Rocha, A. B., Mans, D. R., Regner, A., and Schwartsmann, G. (2002) Targeting protein kinase C: new therapeutic opportunities against high-grade malignant gliomas?, *Oncologist 7*, 17-33.
35. Du, J., Bernasconi, P., Clauser, K. R., Mani, D. R., Finn, S. P., Beroukhim, R., Burns, M., Julian, B., Peng, X. P., Hieronymus, H., Maglathlin, R. L., Lewis, T. A., Liau, L. M., Nghiemphu, P., Mellinghoff, I. K., Louis, D. N., Loda, M., Carr, S. A., Kung, A. L., and Golub, T. R. (2009) Bead-based profiling of tyrosine kinase phosphorylation identifies SRC as a potential target for glioblastoma therapy, *Nat Biotechnol 27*, 77-83.
36. Milano, V., Piao, Y., LaFortune, T., and de Groot, J. (2009) Dasatinib-induced autophagy is enhanced in combination with temozolomide in glioma, *Mol Cancer Ther 8*, 394-406.
37. Roskoski, R., Jr. (2005) Src kinase regulation by phosphorylation and dephosphorylation, *Biochem Biophys Res Commun 331*, 1-14.

606 38. King, C. R., Cohen, M. J., Fonseca, G. J., Dirk, B. S., Dikeakos, J. D., and Mymryk,
607 J. S. Functional and Structural Mimicry of Cellular Protein Kinase A Anchoring
608 Proteins by a Viral Oncoprotein, *PLoS Pathog 12*, e1005621.
609 39. Majewska, E., and Szeliga, M. AKT/GSK3beta Signaling in Glioblastoma,
610 *Neurochem Res 42*, 918-924.
611 40. Mucignat-Caretta, C., Denaro, L., D'Avella, D., and Caretta, A. Protein Kinase A
612 Distribution Differentiates Human Glioblastoma from Brain Tissue, *Cancers*
613 *(Basel) 10*.
614 41. Miyashita, K., Kawakami, K., Nakada, M., Mai, W., Shakoori, A., Fujisawa, H.,
615 Hayashi, Y., Hamada, J., and Minamoto, T. (2009) Potential therapeutic effect of
616 glycogen synthase kinase 3beta inhibition against human glioblastoma, *Clin*
617 *Cancer Res 15*, 887-897.
618 42. Kotliarova, S., Pastorino, S., Kovell, L. C., Kotliarov, Y., Song, H., Zhang, W.,
619 Bailey, R., Maric, D., Zenklusen, J. C., Lee, J., and Fine, H. A. (2008) Glycogen
620 synthase kinase-3 inhibition induces glioma cell death through c-MYC, nuclear
621 factor-kappaB, and glucose regulation, *Cancer Res 68*, 6643-6651.
622 43. Ren, J., Liu, T., Han, Y., Wang, Q., Chen, Y., Li, G., and Jiang, L. GSK-3beta inhibits
623 autophagy and enhances radiosensitivity in non-small cell lung cancer, *Diagn*
624 *Pathol 13*, 33.
625 44. Dedobbeleer, M., Willems, E., Freeman, S., Lombard, A., Goffart, N., and
626 Rogister, B. Phosphatases and solid tumors: focus on glioblastoma initiation,
627 progression and recurrences, *Biochem J 474*, 2903-2924.
628 45. Mui, M. Z., Kucharski, M., Miron, M. J., Hur, W. S., Berghuis, A. M., Blanchette,
629 P., and Branton, P. E. Identification of the adenovirus E4orf4 protein binding
630 site on the B55alpha and Cdc55 regulatory subunits of PP2A: Implications for
631 PP2A function, tumor cell killing and viral replication, *PLoS Pathog 9*, e1003742.
632 46. Mui, M. Z., Zhou, Y., Blanchette, P., Chughtai, N., Knight, J. F., Gruosso, T.,
633 Papadakis, A. I., Huang, S., Park, M., Gingras, A. C., and Branton, P. E. The
634 Human Adenovirus Type 5 E4orf4 Protein Targets Two Phosphatase Regulators
635 of the Hippo Signaling Pathway, *J Virol 89*, 8855-8870.
636 47. Grallert, A., Boke, E., Hagting, A., Hodgson, B., Connolly, Y., Griffiths, J. R.,
637 Smith, D. L., Pines, J., and Hagan, I. M. A PP1-PP2A phosphatase relay controls
638 mitotic progression, *Nature 517*, 94-98.
639 48. Kolupaeva, V., and Janssens, V. PP1 and PP2A phosphatases--cooperating
640 partners in modulating retinoblastoma protein activation, *FEBS J 280*, 627-643.
641 49. Zelenay, S., and Reis e Sousa, C. Adaptive immunity after cell death, *Trends*
642 *Immunol 34*, 329-335.
643 50. Shibutani, S. T., Saitoh, T., Nowag, H., Munz, C., and Yoshimori, T. Autophagy
644 and autophagy-related proteins in the immune system, *Nat Immunol 16*, 1014-
645 1024.
646 51. van den Bossche, W. B. L., Kleijn, A., Teunissen, C. E., Voerman, J. S. A.,
647 Teodosio, C., Noske, D. P., van Dongen, J. J. M., Dirven, C. M. F., and Lamfers,
648 M. L. M. Oncolytic virotherapy in glioblastoma patients induces a tumor
649 macrophage phenotypic shift leading to an altered glioblastoma
650 microenvironment, *Neuro Oncol*.
651 52. Jiang, H., and Fueyo, J. (2014) Healing after death: antitumor immunity induced
652 by oncolytic adenoviral therapy, *Oncoimmunology 3*, e947872.

53. Jiang, H., Rivera-Molina, Y., Gomez-Manzano, C., Clise-Dwyer, K., Bover, L., Vence, L. M., Yuan, Y., Lang, F. F., Toniatti, C., Hossain, M. B., and Fueyo, J. (2017) Oncolytic Adenovirus and Tumor-Targeting Immune Modulatory Therapy Improve Autologous Cancer Vaccination, *Cancer Res 77*, 3894-3907.
54. Kleijn, A., Kloezeman, J., Treffers-Westerlaken, E., Fulci, G., Leenstra, S., Dirven, C., Debets, R., and Lamfers, M. (2014) The in vivo therapeutic efficacy of the oncolytic adenovirus Delta24-RGD is mediated by tumor-specific immunity, *PLoS One 9*, e97495.
55. Vizcaino, J. A., Deutsch, E. W., Wang, R., Csordas, A., Reisinger, F., Rios, D., Dianes, J. A., Sun, Z., Farrah, T., Bandeira, N., Binz, P. A., Xenarios, I., Eisenacher, M., Mayer, G., Gatto, L., Campos, A., Chalkley, R. J., Kraus, H. J., Albar, J. P., Martinez-Bartolome, S., Apweiler, R., Omenn, G. S., Martens, L., Jones, A. R., and Hermjakob, H. (2014) ProteomeXchange provides globally coordinated proteomics data submission and dissemination, *Nat Biotechnol 32*, 223-226.
56. Szklarczyk, D., Morris, J. H., Cook, H., Kuhn, M., Wyder, S., Simonovic, M., Santos, A., Doncheva, N. T., Roth, A., Bork, P., Jensen, L. J., and von Mering, C. The STRING database in 2017: quality-controlled protein-protein association networks, made broadly accessible, *Nucleic Acids Res 45*, D362-D368.
57. Tyanova, S., Temu, T., Sinitcyn, P., Carlson, A., Hein, M. Y., Geiger, T., Mann, M., and Cox, J. The Perseus computational platform for comprehensive analysis of (prote)omics data, *Nat Methods 13*, 731-740.
58. Moritz, C. P. Tubulin or Not Tubulin: Heading Toward Total Protein Staining as Loading Control in Western Blots, *Proteomics 17*.

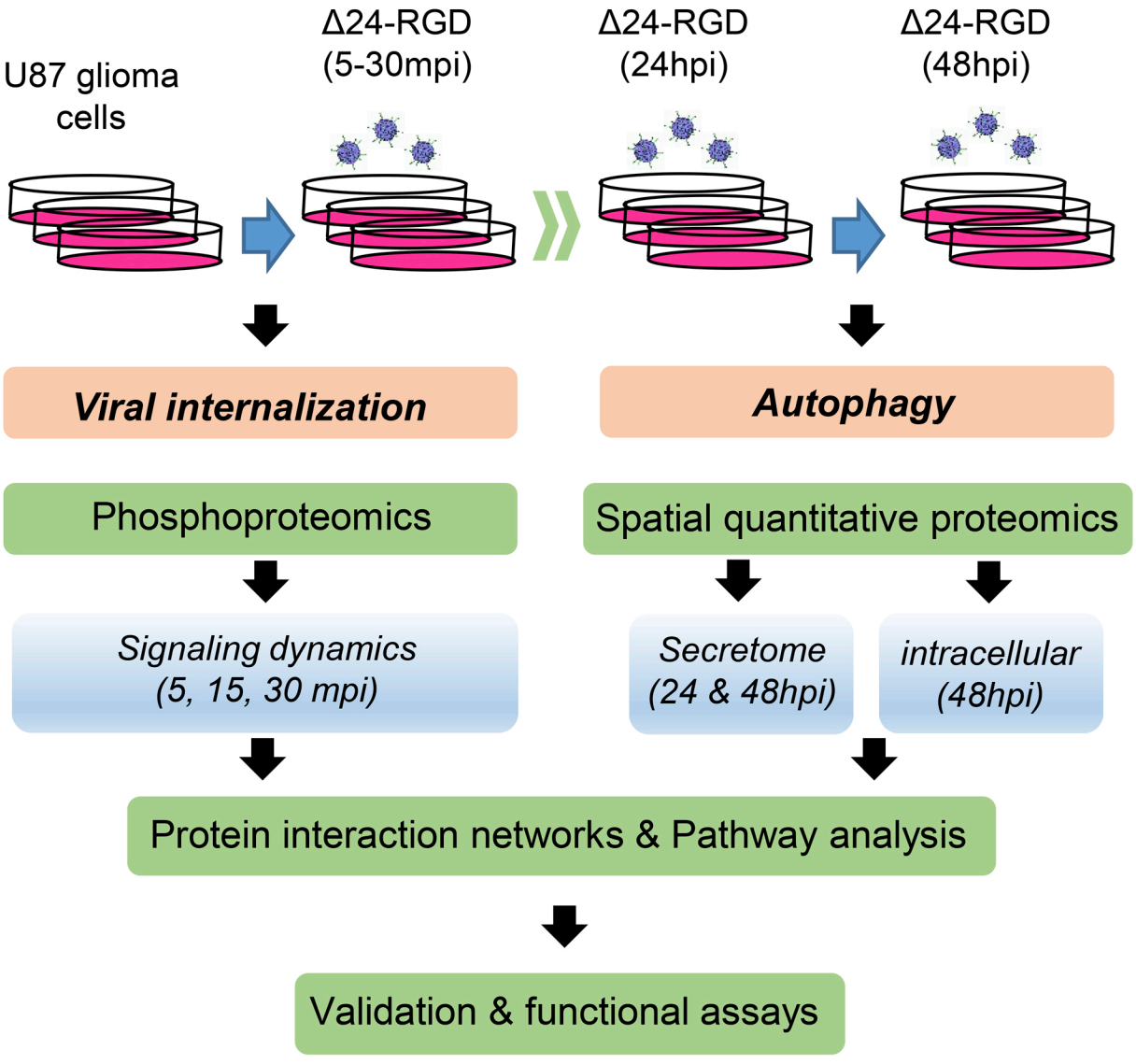
U87 glioma cells
Δ24-RGD (5-30mpi)
Δ24-RGD (24hpi)
Δ24-RGD (48hpi)
Viral internalization
Autophagy
Phosphoproteomics
Spatial quantitative proteomics
Signaling dynamics (5, 15, 30 mpi)
Secretome (24 & 48hpi)
intracellular (48hpi)
Protein interaction networks & Pathway analysis
Validation & functional assays

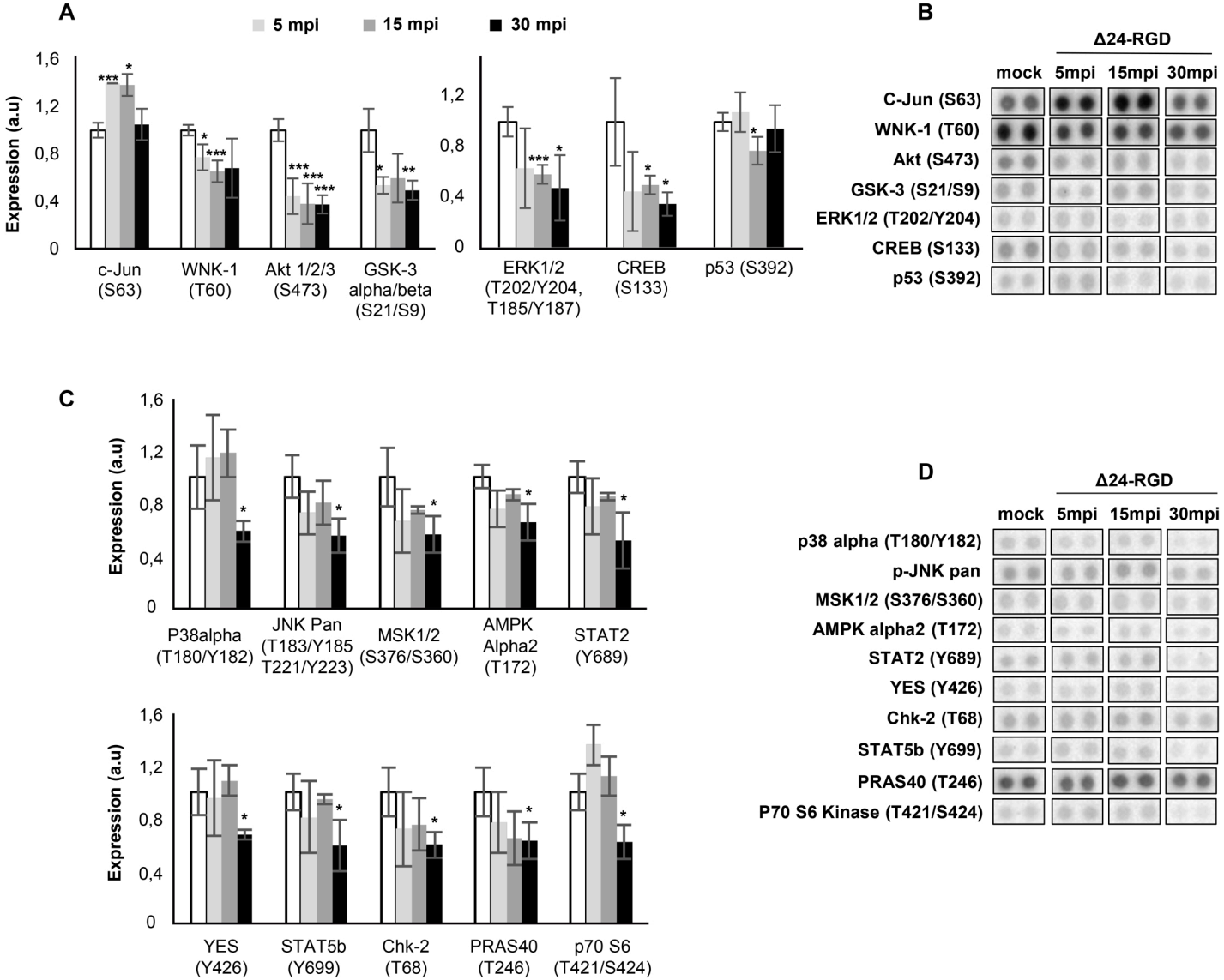
A
5 mpi
15 mpi
30 mpi
Expression (a.u)
1,6
1,2
0,8
0,4
0
c-Jun (S63)
WNK-1 (T60)
Akt 1/2/3 (S473)
GSK-3 alpha/beta (S21/S9)
ERK1/2 (T202/Y204, T185/Y187)
CREB (S133)
p53 (S392)
B
Δ24-RGD
mock
5mpi
15mpi
30mpi
C-Jun (S63)
WNK-1 (T60)
Akt (S473)
GSK-3 (S21/S9)
ERK1/2 (T202/Y204)
CREB (S133)
p53 (S392)
C
P38alpha (T180/Y182)
JNK Pan (T183/Y185 T221/Y223)
MSK1/2 (S376/S360)
AMPK Alpha2 (T172)
STAT2 (Y689)
YES (Y426)
STAT5b (Y699)
Chk-2 (T68)
PRAS40 (T246)
p70 S6 (T421/S424)
D
p38 alpha (T180/Y182)
p-JNK pan
MSK1/2 (S376/S360)
AMPK alpha2 (T172)
STAT2 (Y689)
YES (Y426)
Chk-2 (T68)
STAT5b (Y699)
PRAS40 (T246)
P70 S6 Kinase (T421/S424)

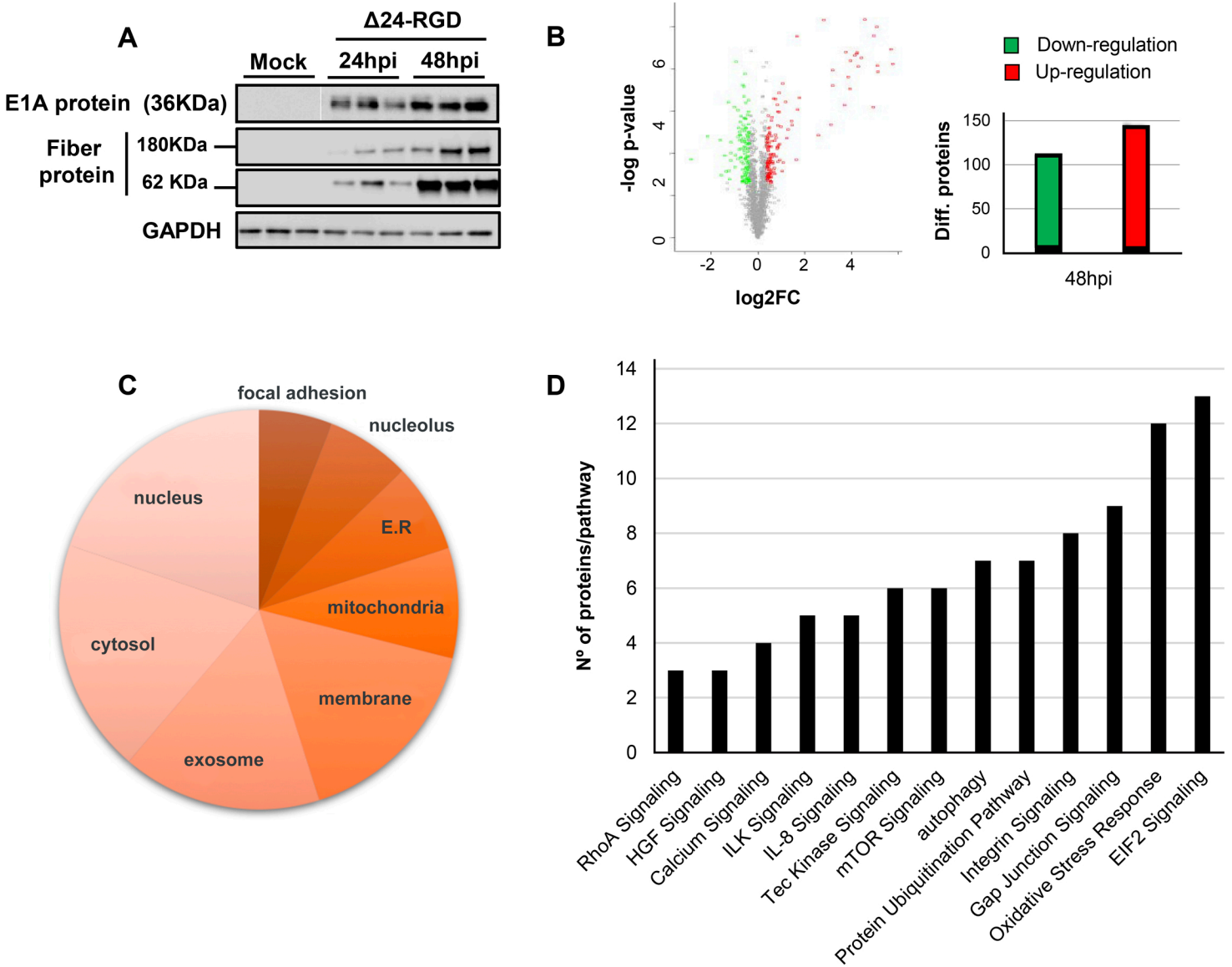
A
Δ24-RGD
Mock
24hpi
48hpi
E1A protein (36KDa)
Fiber protein
180KDa
62 KDa
GAPDH
B
-log p-value
log2FC
Down-regulation
Up-regulation
Diff. proteins
48hpi
C
focal adhesion
nucleolus
nucleus
E.R
mitochondria
cytosol
membrane
exosome
D
Nº of proteins/pathway
RhoA Signaling
HGF Signaling
Calcium Signaling
ILK Signaling
IL-8 Signaling
Tec Kinase Signaling
mTOR Signaling
autophagy
Protein Ubiquitination Pathway
Integrin Signaling
Gap Junction Signaling
Oxidative Stress Response
EIF2 Signaling

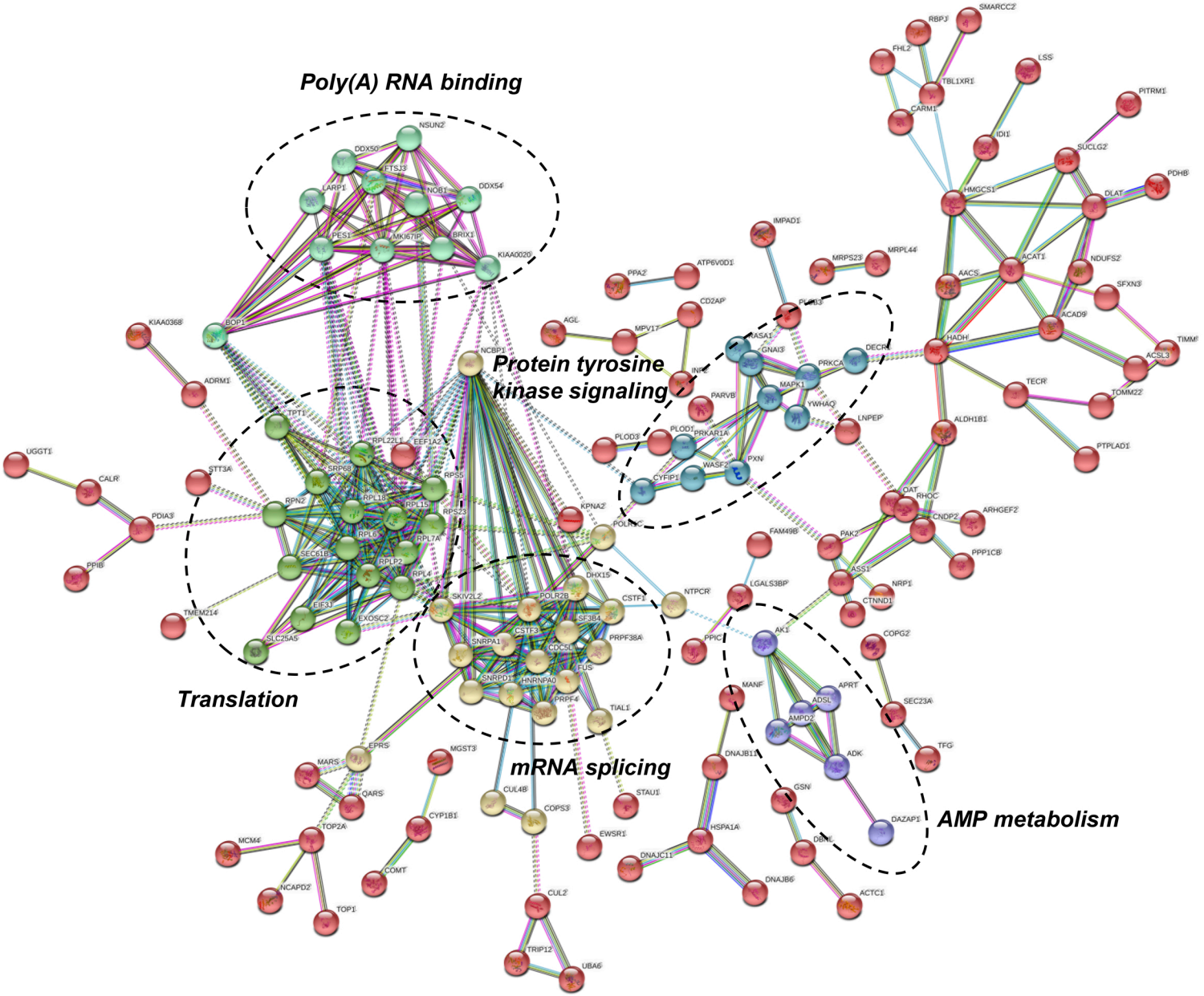
Poly(A) RNA binding
Protein tyrosine kinase signaling
Translation
mRNA splicing
AMP metabolism
NSUN2
DDX50
FTSJ3
LARP1
NOB1
DDX54
PES1
MKI67IP
BRIX1
KIAA0020
BOP1
KIAA0368
ADRM1
NCBP1
TPT1
RPL22L1
EEF1A2
SRP68
RPS5
RPL18
RPL15
RPS23
RPL6
RPL7A
RPL2
RPL4
SEC61B
EIF3J
EXOSC2
SLC25A5
TMEM214
RPN2
PDIA3
CALR
UGGT1
PPIB
STT3A
KPNA2
POLR2C
DHX15
CSTF1
NTPCR
SKIV2L2
POLR2B
SF3B4
CSTF3
PRPF38A
SNRPA1
CDC5L
FUS
SNRPD1
HNRNPA0
PRPF4
TIAL1
EPRS
MARS
QARS
MGST3
CUL4B
COPS3
STAU1
EWSR1
CYP1B1
COMT
TOP2A
MCM4
NCAPD2
TOP1
CUL2
TRIP12
UBA6
IMPAD1
ATP6V0D1
PPA2
CD2AP
AGL
MPV17
PLCB3
INPP4A
PARVB
PLOD3
PLOD1
PRKAR1A
CYFIP1
WASF2
PXN
ASAP1
GNAI3
PRKCA
MAPK1
YWHAQ
LNPEP
DECR1
MRPS23
MRPL44
FAM49B
LGALS3BP
PPIC
AK1
ADSL
AMPD2
APRT
MANF
DNAJB11
HSPA1A
DNAJC11
DNAJB6
GSN
DBNL
ACTC1
DAZAP1
ADK
SEC23A
TFG
COPG2
PAK2
ASS1
CTNND1
NRP1
OAT
RHOC
CNDP2
ARHGEF2
PPP1CB
ALDH1B1
PTPLAD1
TECR
TOMM22
ACSL3
TIMM8
ACAD9
HADH
AACS
ACAT1
NDUFS2
SFXN3
HMGCS1
DLAT
PDHB
SUCLG2
IDI1
CARM1
TBL1XR1
FHL2
RBPJ
SMARCC2
LSS
PITRM1

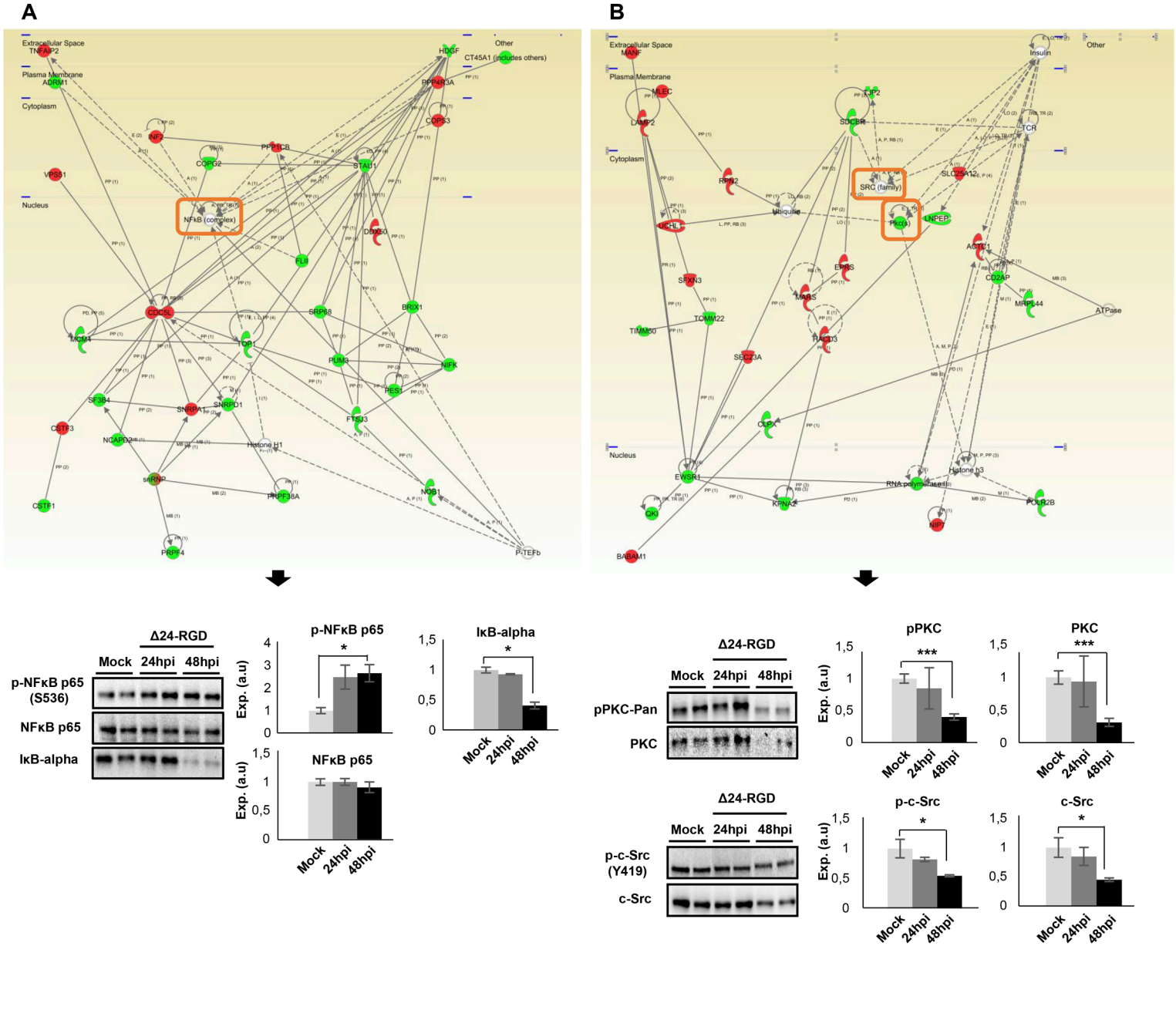
A
B
Extracellular Space
Plasma Membrane
Cytoplasm
Nucleus
Other
NFκB (complex)
SRC (family)
PKC(s)
Δ24-RGD
Mock
24hpi
48hpi
p-NFκB p65 (S536)
NFκB p65
IκB-alpha
p-NFκB p65
IκB-alpha
Exp. (a.u)
pPKC-Pan
PKC
pPKC
PKC
p-c-Src (Y419)
c-Src
p-c-Src
c-Src

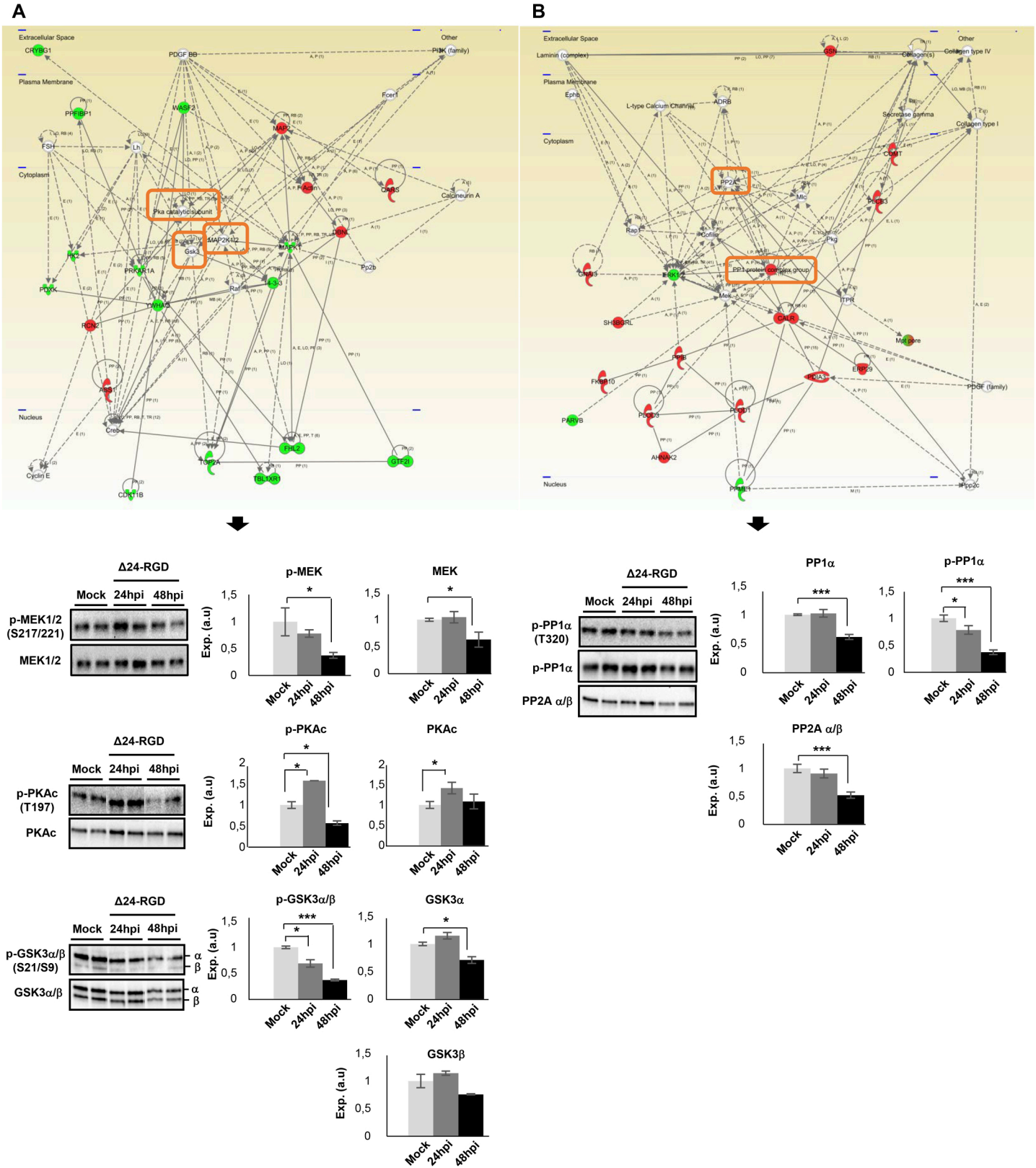
A
B
Δ24-RGD
Mock
24hpi
48hpi
p-MEK1/2 (S217/221)
MEK1/2
p-MEK
MEK
p-PKAc (T197)
PKAc
p-PKAc
PKAc
p-GSK3α/β (S21/S9)
GSK3α/β
p-GSK3α/β
GSK3α
GSK3β
p-PP1α (T320)
p-PP1α
PP2A α/β
PP1α
p-PP1α
PP2A α/β
Exp. (a.u)

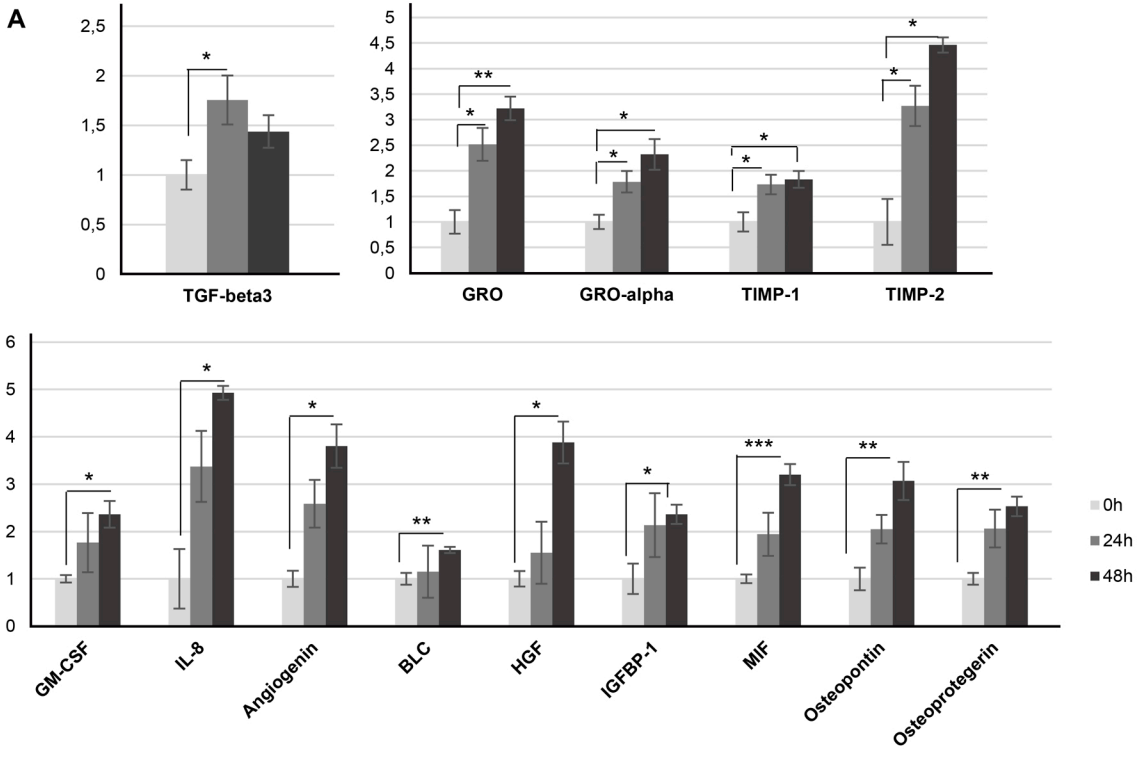
A
TGF-beta3
GRO
GRO-alpha
TIMP-1
TIMP-2
GM-CSF
IL-8
Angiogenin
BLC
HGF
IGFBP-1
MIF
Osteopontin
Osteoprotegerin
0h
24h
48h

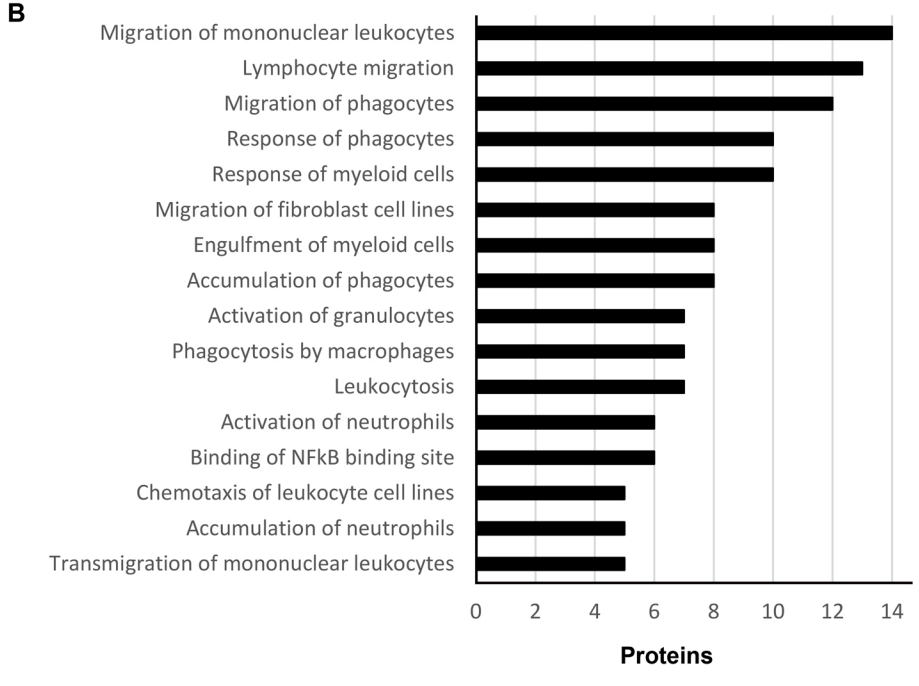
B
Migration of mononuclear leukocytes
Lymphocyte migration
Migration of phagocytes
Response of phagocytes
Response of myeloid cells
Migration of fibroblast cell lines
Engulfment of myeloid cells
Accumulation of phagocytes
Activation of granulocytes
Phagocytosis by macrophages
Leukocytosis
Activation of neutrophils
Binding of NFkB binding site
Chemotaxis of leukocyte cell lines
Accumulation of neutrophils
Transmigration of mononuclear leukocytes
Proteins